



Hybrid PEDOT:PSS to obtain high-performance Ag NW-based flexible transparent electrodes for transparent heaters

Xiaopeng Li¹ · Shihui Yu¹ · Le Zhao¹ · Muying Wu² · Helei Dong³

Received: 20 January 2020 / Accepted: 31 March 2020 / Published online: 4 April 2020
© Springer Science+Business Media, LLC, part of Springer Nature 2020

Abstract

Silver nanowire (Ag NW) networks are remarkable components that may be able to replace indium tin oxide (ITO) as transparent electrodes. In this paper, the Ag NW based flexible transparent electrodes are prepared via PEDOT:PSS sol–gel transition without vacuum process, provides very high figure of merit by minimizing junction resistance, and also exhibit excellent mechanical robustness against bending. The sheet resistance of the flexible Ag NW-based films reduces from 1000 to 9.4 $\Omega/\text{sq.}$ at transmittance of $\sim 90\%$. The conduction mechanism involves Ag NWs to PEDOT:PSS carrier injection prior to the formation of a continuous metal conduction pathway. Calculations of figure of merit display a large value of 340, which is superior to that obtained from the flexible ITO, carbon nanotube, graphene, copper nanowire, and other silver nanowire and hybrid thin films. Meanwhile, the sheet resistance does not show great change after tape test due to the effect of PEDOT:PSS. Finally, the successful implementation of the prepared Ag NWs-based transparent electrodes into a flexible transparent heater is demonstrated, verifying the applicability of the electrodes. It is believed that our study is the key step toward realizing the practical use of NW flexible transparent electrodes in various flexible electronic devices.

1 Introduction

Flexible transparent conductive electrodes (FTCEs) are widely used in organic solar cells, organic light-emitting diodes (OLEDs), touch screens, flexible transparent heaters and many other flexible optoelectronic devices [1–3]. Indium tin oxide (ITO) thin films are commonly used as transparent conductive electrodes but its usage in flexible substrates is highly limited because of the fragile ceramic nature and damage of organic substrates during high-temperature processing conditions [4, 5]. Therefore, several alternatives have been proposed including

graphene [6], carbon nanotubes (CNT) [7], metal meshes [8, 9], conductive polymers [10] and metallic nanowires [11, 12]. Among those candidates, FTCEs based on metallic nanowires (NWs) have received increasing much scientific attention as an essential component for various applications in the next-generation future electronic components [12, 13]. Especially, silver nanowire (Ag NW) thin films exhibit a great potential for the devices due to low conductivity (15–25 $\Omega/\text{sq.}$), good flexibility and high transmissivity (80–90%) in the visible spectrum [13, 14]. Furthermore, Ag NW thin films can be easily prepared for large-scale devices by solution-based processes [15]. Unfortunately, compared with the rigid ITO on glass (sheet resistance $\sim 10 \Omega/\text{sq.}$, transmittance $\sim 85\%$) [16, 17], the optical and electronic properties of Ag NW-based FTCEs still perform poorly. To further enhance the performances of Ag NW thin films, some researchers have reported novel approaches including tuning the length-to-diameter ratio by optimizing the Ag NW synthesis process [18], directional arrangement of NWs [11], and welding of junctions [19]. However, there are also some severe drawbacks of as-prepared Ag NWs based FTCEs including weak mechanical adhesion to the substrate and relatively higher resistance due to high interwire contact resistance [20]. In addition, the complex processing conditions of

✉ Shihui Yu
ysh728@126.com

✉ Helei Dong
donghelei@nuc.edu.cn

¹ School of Microelectronics and Tianjin Key Laboratory of Imaging and Sensing Microelectronic Technology, Tianjin University, Tianjin 300072, People's Republic of China

² School of Electronic Engineering and Intelligentization, Dongguan University of Technology, Dongguan 523808, Guangdong, China

³ School of Instrument and Electronics, North University of China, Taiyuan 030051, China

directional arrangement and junction welding limit the practical application of Ag NWs. Therefore, an effective and simple method is necessary to develop composite electrode for overcoming the above intrinsic problems of Ag NW-based FTCEs.

Recently, metal-oxide layers have been introduced to enhance the adhesion of the Ag NW-based FTCEs to the substrate [21–23]. These present methods to improve the conductivity of Ag NW-based FTCEs need to rely on vacuum processing, or enhance the adhesion sacrificing conductivity/translucency. The method enhancing both of the adhesion and conductivity of Ag NW-based FTCEs with a high transmittance via a simple process is very limited. Poly(3, 4-ethylenedioxythiophene): poly(styrene sulfonate) (PEDOT:PSS) is the widely used and commercially available conductive polymer [24, 25], and it possesses unique features such as high mechanical flexibility, improved mechanical adhesion to the substrate and easy solution-based processability [26, 27]. Hence, we propose to improve the performance of Ag NW based FTCEs by adhesion engineering via PEDOT:PSS gel. We suggest that the connection of junctions between the Ag NWs by PEDOT:PSS can reduce interwire contact resistance, leading to the improvement of conductivity and mechanical adhesion without deterioration of transmittance. Moreover, the enhanced adhesion in turn further improves the conductivity of Ag NW networks owing to the downward force from the adhesive gel to Ag NWs. In this paper, a fully indium-free and vacuum-free process newly designed FTCEs based on effective PEDOT:PSS adhere to Ag NW networks is demonstrated. The Ag NWs based FTCEs exhibit a low sheet resistance of 9.4 Ω /sq and a high transmittance of 89.2%. Importantly, they also show an increase of less than 35% after tape cycles (30 times) and bending cycles (2000 times) with good solvent-resistance.

2 Experimental section

2.1 Synthesis of Ag NWs

Silver nanowires were fabricated using a modified polyol reduction. Add 0.1 g of PVP to 25 ml of EG, completely dissolved it by magnetic stirring, then add 0.35 g of AgNO_3 to the PVP/EG solution. After it is completely dissolved, 4 ml of FeCl_3 solution (the amount of the substance in the EG solution is 600 μM) was added, and after stirring for 1 min, the mixed solution was transferred to the hydrothermal synthesis reactor, and the reaction was carried out in a hot air circulation drying oven at 150 $^\circ\text{C}$ for 10 h and then cooled to room temperature. The solution was then centrifuged (1 time at 2000 rpm) to remove EG, PVP, and other impurities

from the supernatant after adding ethanol. The Ag NWs were suspended in ethanol at a concentration of 2 $\text{mg}\cdot\text{mL}^{-1}$.

2.2 Fabrication of Ag NW-based FTCEs

The PET substrate was ultrasonically washed with absolute ethanol and deionized water, and dried with high-purity nitrogen gas for use. PEDOT:PSS was mixed with deionized water, absolute ethanol, and ethylene glycol at 1:0.5:0.3:0.2, and sonicated for 20 min. The bottom layer PEDOT:PSS solution gel was spin-coated on PET substrates at 6000 rpm for 60 s, then placed in an oven at 80 $^\circ\text{C}$ for 2 min, the thickness was ~ 15 nm. The silver nanowires were spin-coated on the PEDOT:PSS layers at 1000 rpm for 60 s. The density of Ag NW networks was controlled via the number of spins which varied between 1 and 5. Finally, the PEDOT:PSS solution was coated on the Ag NWs by spin coating technique, the spin speed of coating was 5000 rpm, and the time was 60 s. After the spin coating was completed, it was baked in an oven at 150 $^\circ\text{C}$ for 30 min. For comparison, the as-prepared Ag NW networks with various number of spins were deposited on the PET substrates as well.

2.3 Characterization

The surface micrograph was obtained via field emission scanning electron micrograph (FE-SEM, JEOL JSM-6701 F). The optical photographs and micrographs were obtained using iPhone 6 s plus mobile phone and optical microscope. The surface roughness was obtained via the measurement of profilometer (Alpha-Step D-100, KLA-Tencor, California, USA). The structure was characterized by X-ray diffraction (Rigaku D/MAX-RB, Akishima, Tokyo, Japan). Optical transmittance spectra were characterized by ultraviolet visible (UV–Vis) spectrophotometer (Varian Cary 5000). The sheet resistance was obtained via the four-point probe instrument (SX1934, SuZhou, P.R. China). The flexibility tests were performed using a homemade instrument that had a bending radius of ~ 3 mm and a bending speed of one cycle per second. The adhesive tests were done by 3 M scotch tape: A 10 mm-wide 3 M scotch tape was attached to the sample, and then slowly peeled off from the sample.

2.4 Fabrication of flexible transparent heater

Two silver-epoxy adhesive lines were brushed at the edges of a square sample as contacts. DC bias voltage was supplied to the flexible transparent heater through a programmable DC power supply (eTM-L303SPL, eTOMMENS, Shenzhen, China), and a GDM-8352 digital multimeter (Gwinstek, Taiwan, China) coupled with a thermal resistance was used to monitor the temperature of the flexible transparent heater.

The infrared image was recorded by an infrared thermal imager (HT18, XINTEST, Ltd, Shenzhen, China).

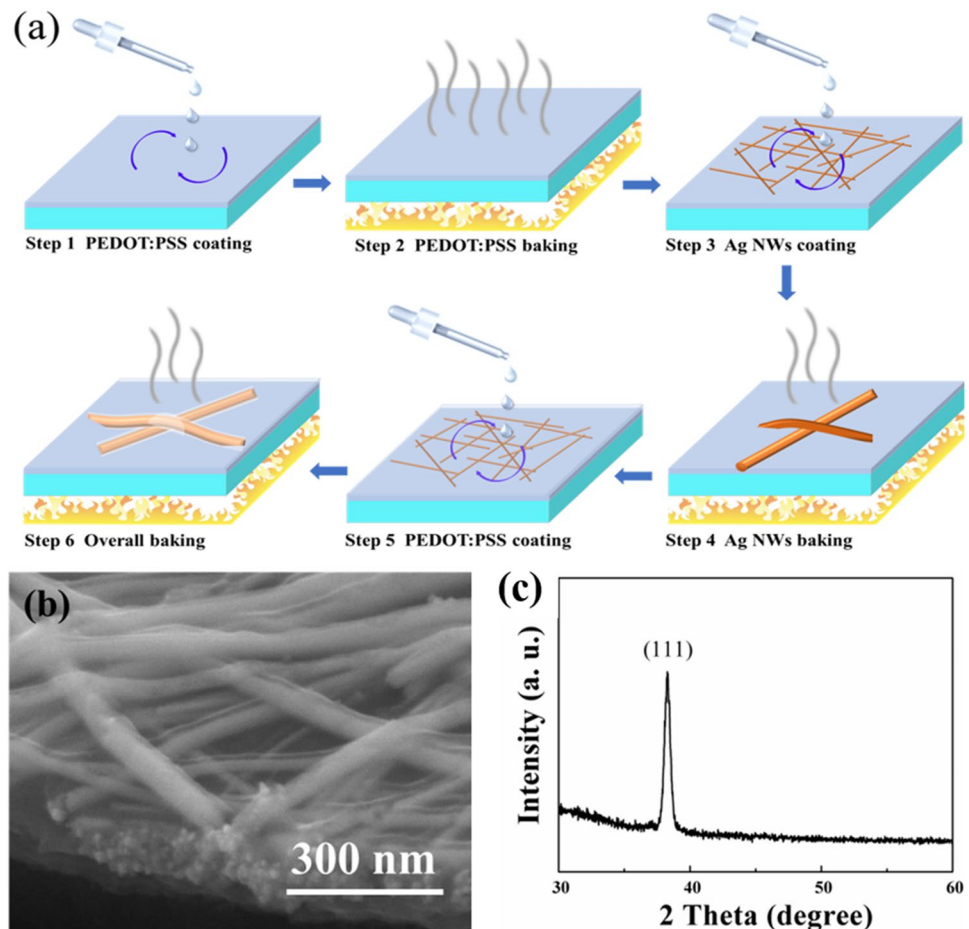
3 Results and discussion

The fabrication procedure of the Ag NWs/PEDOT:PSS hybrid thin films on the PET substrates can be seen in scheme Fig. 1a, as described in the Experimental section. First, 15 nm thick PEDOT:PSS adhesive layers are spin-cast on a clean bare PET substrate (step 1), followed by heating for 10 min at 80 °C lead to the evaporation of water and alcohol in PEDOT:PSS (step 2). In step 3, Ag NWs dispersion in ethanol are spin-coated on the surface of PEDOT:PSS /PET. Subsequently, Ag NWs are dried at 60 °C in air for 5 min (step 4). In step 5, PEDOT:PSS solution is coated on the surface of Ag NW networks. At last, Ag NWs/PEDOT:PSS hybrid thin films are heated at 150 °C for 30 min in air. The density of Ag NWs on the PET substrates can be easily controlled via the number of coating cycles and the spin-coating speed. Figure 1b displays the cross-section FESEM micrographs of the Ag NWs/PEDOT:PSS hybrid thin films. When the PEDOT:PSS is stuck to the Ag NW networks, the

neighboring crossed Ag NWs can naturally coalesce together driven by surface tension, therefore, the good electrical conductivity can be achieved. In addition, the bottoms of Ag NWs are buried in the bottom PEDOT:PSS layers enhancing the adhesive capacity. Figure 1c shows the XRD spectra of as-prepared Ag NW thin films on PET substrates. There is only a strong (1 1 1) peak in addition to PET substrate peaks, indicating that the Ag NWs have a crystalline structure with a strongly (1 1 1) preferred orientation and do not contain other impurities.

Figure 2a and b show the FE-SEM micrographs of as-prepared Ag NW thin films with various number of spin-coating cycles. The Ag NW networks with one spin-coating cycle exhibit a lower density than the with five spin-coating cycles. The density of the Ag NW networks is dependent on the spin-coating cycles. It is noticeable, however, the Ag NW networks have a poor-connected wire–wire junction owing the inherent characteristic of Ag NWs. Figure 2c shows the sheet resistance and optical transmittance (at 550 nm) of as-prepared Ag NW thin films with various number of spin-coating cycle. The one spin-coated Ag NW networks show a fairly high sheet resistance of $\sim 950 \Omega/\text{sq}$ because of the low density of Ag NWs as well as the randomly unconnected

Fig. 1 **a** Schematic illustration of the fabrication process. **b** Cross-section FE-SEM micrographs of the Ag NWs/PEDOT:PSS hybrid thin films. **c** XRD spectra of as-prepared Ag NW thin films on PET substrates



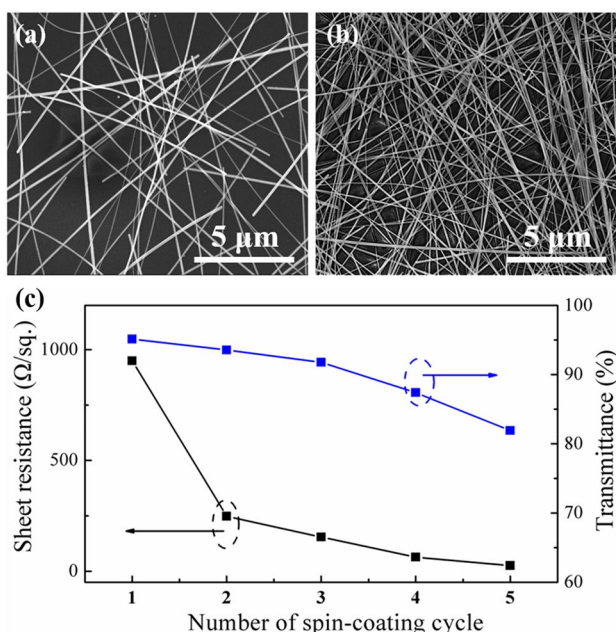
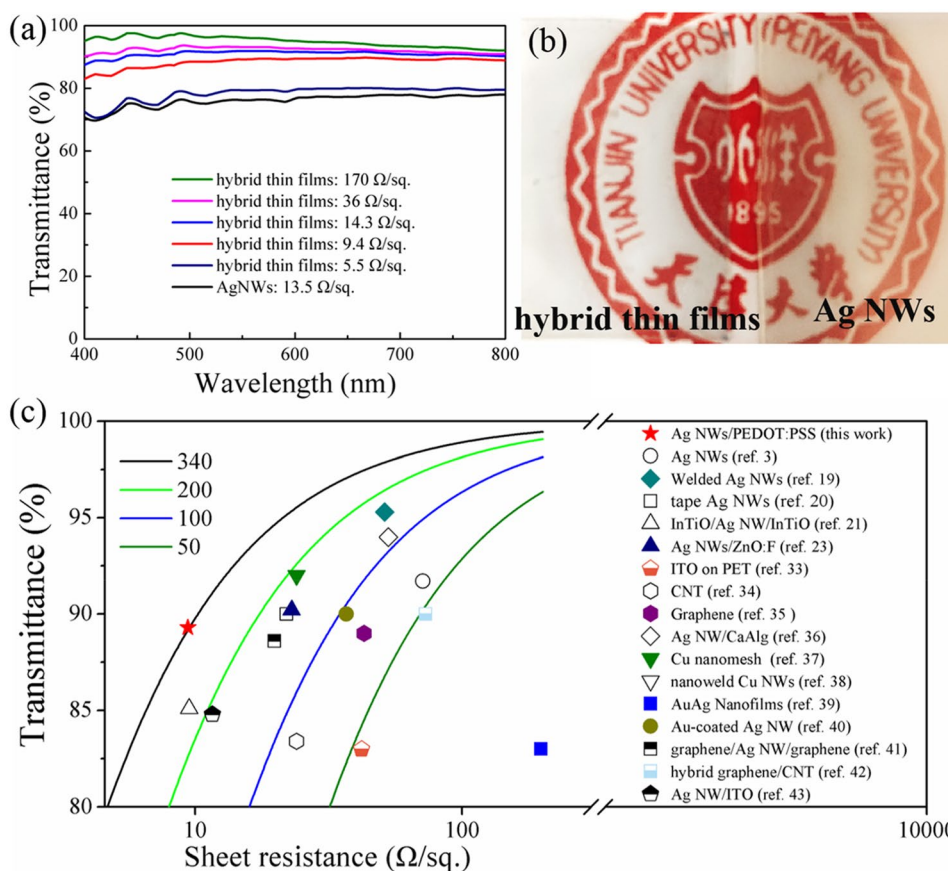


Fig. 2 **a** FE-SEM micrographs of as-prepared Ag NW thin films with one spin-coating cycle and **b** five spin-coating cycles. **c** sheet resistance and optical transmittance (at 550 nm) of as-prepared Ag NW thin films with various number of spin-coating cycle

wire–wire contacts (see the Fig. 2a). As the spin-coating cycles increase to five times, the sheet resistance decreases significantly from ~950 to ~25 Ω/sq, which can be due to the increase in Ag NW density (see the Fig. 2b). Correspondingly, the optical transmittance, like the sheet resistance also reduces drastically from 95.1 to 81.9% with the spin-coating cycle increasing from one to five times, due to the light scattering in the random Ag NW networks.

By optimizing the spin-coating process conditions of PEDOT:PSS solution, the highly opto-electrical Ag NWs/PEDOT:PSS hybrid thin films are prepared on PET. Figure 3a exhibits the optical transmittance spectra (400–800 nm) of the Ag NWs/PEDOT:PSS hybrid thin films with varying sheet resistance values. The hybrid thin films show a fairly high transparency performance, and the transmittances of hybrids are nearly constant in the visible light range. The transmittance is about 96.2% at 550 nm wavelength for a 170 Ω/sq, 93.1% for a 36 Ω/sq, 91.9% for a 14.3 Ω/sq, 89.2% for a 9.4 Ω/sq and 79.3% for a 5.5 Ω/sq hybrid thin films. Generally, higher transmittance means lower Ag NW density on the PET, leading to larger sheet resistance. And, more remarkable the hybrid thin films display excellent conductivity compared to as-prepared Ag NW thin films. Figure 3b exhibits the visual effect of optical transparency for as-prepared Ag NW and Ag NWs/

Fig. 3 **a** Optical transmittance spectra (400–800 nm) of the Ag NWs/PEDOT:PSS hybrid thin films with varying sheet resistance values. **b** Visual effect of optical transparency for as-prepared Ag NW and Ag NWs/PEDOT:PSS hybrid thin films. **c** Optical transmittance of Ag NWs/PEDOT:PSS hybrid thin films as a function of sheet resistance (in comparison to Ag NWs [3], welded Ag NW [19], tape Ag NWs [20], InTiO/Ag NW/InTiO [21], Ag NWs/ZnO:F [23], ITO on PET [32], CNT [33], graphene [34], Ag NWs/CaAlG [35], Cu nanomesh [36], nanoweld Cu NWs [37], AuAg nanofilms [38], Au coat Ag NW [39], graphene / Ag NW/ graphene [40], hybrid graphene/CNT [41], and Ag NW/ITO [42]). The solid lines represent Eq. (1) for the given values of *F*



PEDOT:PSS hybrid thin films on the PET substrate at the equivalent sheet resistance of $\sim 9.0 \Omega/\text{sq}$. It can be clearly seen from the figure (insignia of Tianjin University) that the Ag NWs/PEDOT:PSS hybrid thin films have a higher transmittance than the as-prepared Ag NWs.

The common FoM (F) is utilized to evaluate the optimal trade-off between the optical and electronic properties better. The F value, namely the ratio of electrical conductance to optical conductance ($\sigma_{\text{dc}}/\sigma_{\text{opt}}$), can be defined via using the following expression [28, 29]:

$$\frac{\sigma_{\text{dc}}}{\sigma_{\text{opt}}} = \frac{Z_0}{2R_{\text{sh}}} \frac{\sqrt{T_{\text{av}}}}{1 - \sqrt{T_{\text{av}}}} \quad (1)$$

$$F = \frac{\sigma_{\text{dc}}}{\sigma_{\text{opt}}} \quad (2)$$

where σ_{dc} defines the DC conductivity of the thin films, σ_{opt} defines the optical conductivity at wavelength of λ nm, Z_0 defines the impedance of free space (377Ω) and R_{sh} defines the sheet resistance. Hu et al. [29] first used the expression for estimating the performance in CNT FTCEs, then the expression is used extensively in lots of different TCEs, and F value is more useful in comparing transparent conducting thin films [1, 30]. In Fig. 3c, to fit the data, four different F values (340, 200, 100, and 50, the dashed line in Fig. 3c) are used. Our Ag NWs/PEDOT:PSS hybrid thin films have good performance with low sheet resistance ($9.4 \Omega/\text{sq}$) and high transmittance (89.2%) with $F = 340$. Figure 3c shows the comparisons of optical transmittance and sheet resistance of our Ag NWs/PEDOT:PSS hybrid thin films with commercial ITO on PET ($F = \sim 50$) [31, 32], carbon nanotube ($F = 60\text{--}80$) [7, 33], graphene ($F = \sim 48$) [6, 34], and silver nanowire ($F = 100\text{--}240$) [3, 10, 19, 20, 35], copper nanowire ($F = 25\text{--}230$) [36, 37], and hybrid transparent conductive thin films ($F = 10\text{--}260$) [21, 23, 38–42]. The Ag NWs/PEDOT:PSS hybrid thin films (Ag NWs spin-coating cycles = 4) exhibit higher F value than those of the reference TCEs. With this exceptional opto-electrical performance, the Ag NWs/PEDOT:PSS hybrid thin films can be suitable for high-performance optoelectronic device applications.

The PEDOT:PSS consolidates the contact of Ag NWs, similar to the effect of high-temperature welding. The effect can be varied by the analysis of the FE-SEM micrographs changes on the Ag NW surfaces. Figure 4a and b show the FE-SEM micrographs of two junctions for the as-prepared Ag NW and Ag NWs/PEDOT:PSS hybrid thin films. For the as-prepared Ag NW thin films (as shown in Fig. 4a), every Ag nanowire is located lightly on the neighboring Ag NWs or PET substrate with limited point contact or line contact. After the addition of PEDOT:PSS (as shown in Fig. 4b), it is clearly shown

that the Ag NWs are wrapped tightly into a well-formed PEDOT:PSS layer, sharp micrographs with clear thick sides are always observed at crossed Ag NWs position of Ag NWs/PEDOT:PSS hybrid thin films (inset of Fig. 4b), the wire–wire junction gap is drastically declined or even disappeared and contact area is enlarged. Figure 4c and d show the schematic of the effect of PEDOT:PSS on Ag NW junctions. In the as-prepared Ag NW thin films, a higher interwire contact resistance resulting from a weak nanowire–nanowire connection leads to a relatively worse conductivity. After applying PEDOT:PSS, the junctions of Ag NWs are strongly contacted owing to the downward force exerted by the PEDOT:PSS solution between Ag NWs and PET substrate. Therefore, the interconnection in Ag NWs is improved, leading to the improvement of the interwire contact conductivity and reduction of the overall resistance for the hybrid thin films. In addition, the PEDOT:PSS is P-type semiconductor material, its work function (ϕ_{p}) is 4.8–4.9 eV [43, 44], which is lower than that of Ag NWs ($\phi_{\text{A}} = 5.0\text{--}5.1$ eV) [45, 46], resulting in the ohmic contact formation between PEDOT:PSS and Ag NWs. Figure 4e–g display the schematic diagrams of the energy band structures that can be expected prior to and after PEDOT:PSS and Ag NWs are brought into contact, respectively. The as-prepared Ag NW networks have a high contact resistance between Ag NWs. After the PEDOT:PSS contact with the Ag NWs, the junctions between Ag NWs are connected by PEDOT:PSS, as shown in Fig. 4b and d. At this time, a great deal of electrons from the Ag NWs inject straight into the PEDOT:PSS because of the difference of work functions between them, resulting in the accumulation of numerous electrons in a very small region near the interface. Due to the transfer of electrons, both the valence and conduction bands of PEDOT:PSS are curved upward. When a thermodynamic equilibrium is received, the Fermi level across interface the in a straight line at this moment, as shown in Fig. 4g. The barrier between PEDOT:PSS and Ag NW interfaces disappear, a great deal of electrons in the Ag NW flows into PEDOT:PSS in the meantime. Therefore, the significant electronic transmission channels between Ag NWs are provided, leading to a decrease of contact resistance. As a consequence, the sheet resistance of Ag NWs/PEDOT:PSS hybrid thin films further decrease, due to the resulting effect on the PEDOT:PSS conduction path. These phenomena are consistent with the results revealed in Fig. 4b.

In addition to the excellent transparency and conductivity, the Ag NWs/PEDOT:PSS hybrid thin films in this study show outstanding toughness as well. The as-prepared Ag NW and Ag NWs/PEDOT:PSS hybrid thin films are subjected to an adhesion test using a 3 M tape (Scotch Magic 810 tape). The fresh 3 M tape is attached to the samples and

Fig. 4 FE-SEM micrographs of **a** as-prepared Ag NW thin films and **b** Ag NWs/PEDOT:PSS hybrid thin films. **c** and **d** Schematic diagrams of Ag NWs on PET corresponding to **a** and **b**. **e** Energy band diagrams of Ag NW and PEDOT:PSS. **f** Schematic band diagram of the as-prepared Ag NW thin films and **g** Ag NWs/PEDOT:PSS hybrid thin films

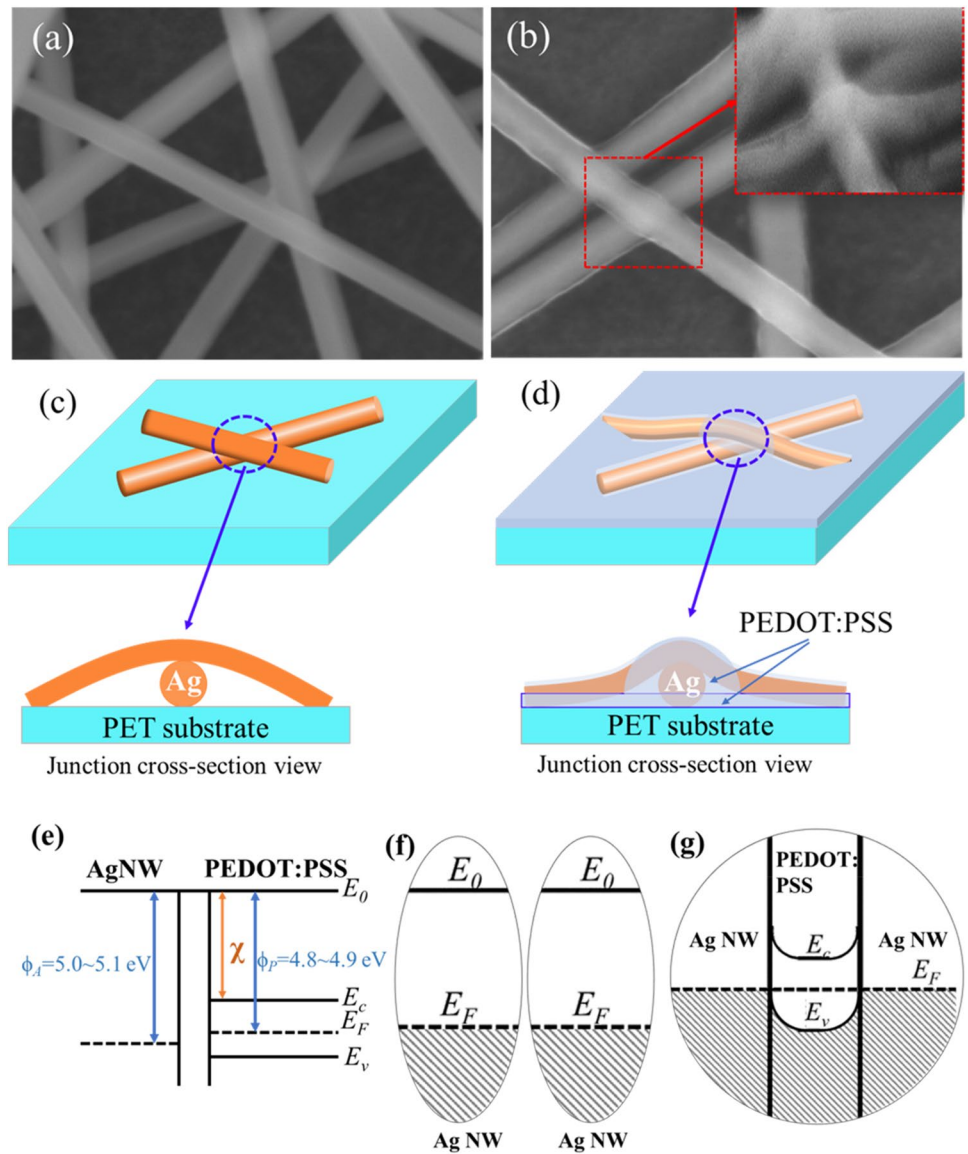
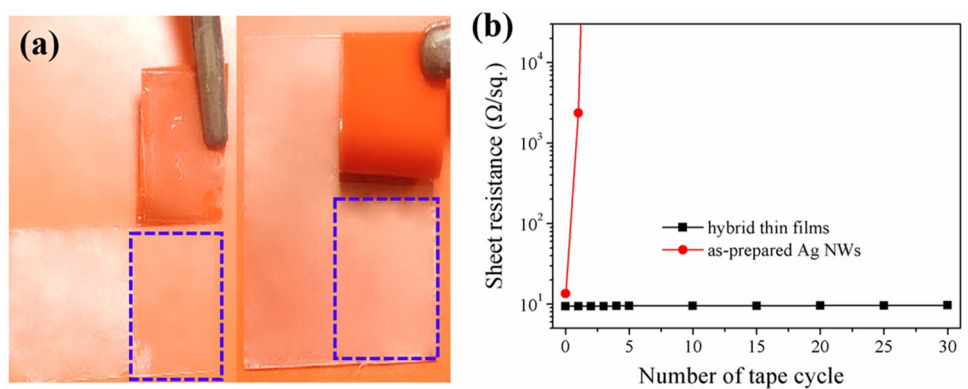


Fig. 5 **a** Adhesion test images of as-prepared Ag NW and Ag NWs/PEDOT:PSS hybrid thin films. The blue rectangles indicate the area where the peeling tests were applied. **b** Sheet resistance as a function of the number of peeling tests for the as-prepared Ag NW and Ag NWs/PEDOT:PSS hybrid thin films

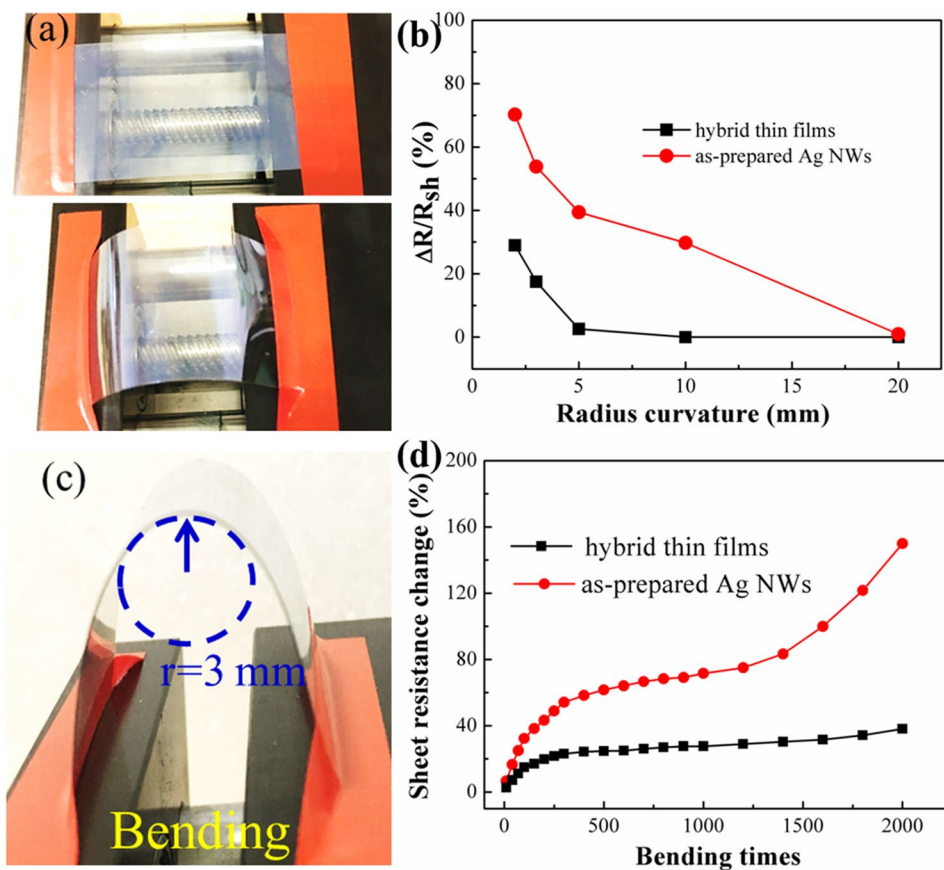


then is peeled off by hand. Figure 5a shows the photographs of as-prepared Ag NW and Ag NWs/PEDOT:PSS hybrid thin films before and after tape test. The as-prepared Ag NW thin films are known to be easily detached from the PET by tape due to its loose adhesion to the substrates. A clear boundary near the dotted blue line on the left side of Fig. 5a can be seen after tape test. However, there is no appreciable variation in visual appearance for the Ag NWs/PEDOT:PSS hybrid thin films after tape test, indicating significantly enhanced adhesion of Ag NWs to the PET substrates. The sheet resistances of as-prepared Ag NW and Ag NWs/PEDOT:PSS hybrid thin films with various tape cycles are shown in Fig. 5b. The sheet resistance of the hybrid thin films is monitored throughout the taping and peeling process, indicating that there is no significant variation on the conductivity of the FTCEs after 30 cycles of taping and peeling. In contrast, the as-prepared Ag NW thin films lost their electrical conductivity at twice due to the fact that the samples are completely delaminated from the PET substrates (as shown in Fig. 5a). The mean surface roughness of the as-prepared Ag NW thin films is ~ 50 nm, while the that of hybrid thin films is ~ 25 nm, which forebodes that the bottom parts of Ag NWs are partially embedded in PEDOT:PSS layer for the hybrid thin films (as shown in Figs. 1b and 4d).

This is the crucial reason for the strong adhesion of Ag NWs to PET substrates.

Ag NW thin films are recognized as a promising FTCE due to their outstanding bending properties. To compare the flexibility of the two kinds of thin films in this work, the as-prepared Ag NW and Ag NWs/PEDOT:PSS hybrid thin films are evaluated in various bending tests. In the bending test, the samples are fixed between two adhesive tapes and then bent by pushing the two clamps together (as shown in Fig. 6a). Figure 6a shows a photograph of the Ag NWs/PEDOT:PSS hybrid thin film on a PET substrate, demonstrating its flexibility and transparency. Figure 6b shows the sheet resistance with the change of bending radius for as-prepared Ag NW and Ag NWs/PEDOT:PSS hybrid thin films. The sheet resistance of hybrid thin films is measured throughout the test and do not change over 10% when the bending radius changes from 20 to 3 mm. In comparison, the sheet resistance of as-prepared Ag NW thin films changes above 50% when the bending radius is 3 mm. The repeated fatigue bending test is performed in which the samples are repeatedly bent at a radius of curvature of 3 mm (Fig. 6c, bottom). The nominal bending strain of Ag NWs/PEDOT:PSS hybrid thin films can be calculated as follows [47]:

Fig. 6 **a** Photograph of the bending test machine used in this study. **b** Sheet resistance changes ($\Delta R/R_0$) of as-prepared Ag NW and Ag NWs/PEDOT:PSS hybrid thin films under various bending radius. **c** Photograph of a flexible and transparent Ag NWs/PEDOT:PSS hybrid thin films on a PET substrate and schematics showing the mechanical bend test conditions. **d** Sheet resistance changes ($\Delta R/R_0$) of during the bend test for the as-prepared Ag NW and Ag NWs/PEDOT:PSS hybrid thin films



$$\epsilon_f = \frac{d}{2r} \tag{3}$$

where, ϵ_f is the nominal bending strain, d is the thickness of PET, and r is the radius of curvature. According to the Eq. (3), the typical bending strain is calculated as 2.5%. The variation of sheet resistance during the repetitive bending is represented by the following equation:

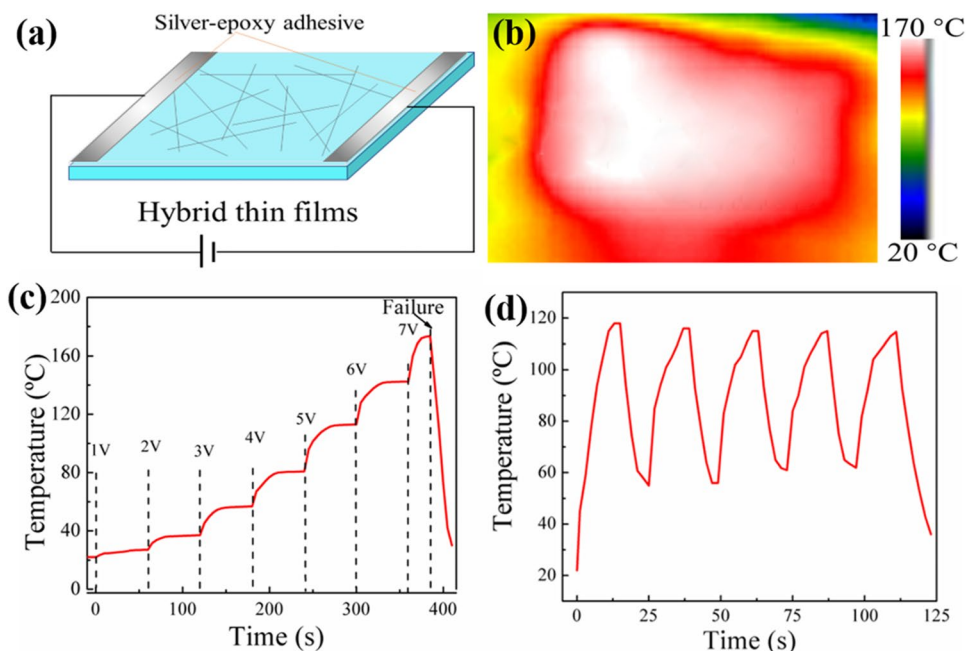
$$R_s = \frac{\Delta R}{R_{sh}} \times 100\% = \frac{(R_c - R_{sh})}{R_{sh}} \times 100\% \tag{4}$$

where, R_s is the change rate of sheet resistance, ΔR is the variation of sheet resistance after bending cycles, R_{sh} and R_c are the initial sheet resistance and measured sheet resistance after bending cycles, respectively. As shown in Fig. 6d, the sheet resistance of the as-prepared Ag NW thin films dramatically increases after 100 bending cycles (the change rate is above 40%), and steadily increases during 2000 bending cycles. Finally, the change rate of sheet resistance at 2000 bending cycles reaches almost 150% for the as-prepared Ag NW thin films. When the as-prepared films are bent, Ag NWs are stretched to some extent or even broken after bending, resulting in an obvious drop in electrical conductivity. In stark contrast, the sheet resistance of the hybrid thin films slightly increased less than 10% from its initial value after 100 cycles of tensile and compression folding. Change rate of sheet resistance increases to 40% at 2000 bending cycles. It is notable that the Ag NWs/PEDOT:PSS hybrid thin films show a high tolerance to bending stress compared to the as-prepared Ag NW thin films.

A flexible transparent heater (FTH) is prepared as an emerging application to demonstrate the feasibility of Ag

NW based FTCE in this work. Constant DC bias voltage is applied between two side ends of the FTH to induce electrically driven resistive Joule heating [48] (as shown in Fig. 7a), and the voltage is raised by 1 V every 60 s until the FTH fails. The temperature is read every second via an infrared thermal camera at a fixed distance of 5.0 cm. Thanks to the uniform distribution realized by the spin-coating, the FTHs shows a uniform temperature distribution (as shown in Fig. 7b). Therefore, the average temperature instead of a maximum temperature is used to evaluate the FTHs' performance. Figure 7c shows the time dependent average temperatures at different DC bias voltage. According to the Joule law, the power dissipated (P) of resistive conductor is defined as $P = V^2/R$, where V denotes the bias voltage. That is to say, higher heat dissipation can be achieved at lower resistance at a fixed voltage. With the bias voltage increases in 1 V increments, the temperature increases rapidly and then reaches the saturation value within 10 s. The FTH fails at 7 V, and the local temperature exceeds 190 °C can be conjectured at 8 V based on the extrapolation from preceding data. The upper working temperature (~165 °C) of PET limits the higher temperature for FTH. Fortunately, the operating temperature of wearable applications is much lower (≤ 75 °C) [49], so the thermal stability of the FTH is estimated to be suited to wearable electronics applications. Figure 7d shows the on/off responses of the FTH at DC bias voltage of 5 V. The heating and cooling time in each cycle is 13 and 12 s, respectively, and the saturation temperature is always around 115 °C. It was confirmed that there are no significant variation in temperature, nor performance decrease in repeated heating tests for 10 times, indicating that the quick response and stable temperature recoverability

Fig. 7 **a** Schematic illustration of a film heater based on the Ag NWs/PEDOT:PSS hybrid thin films. **b** Thermographic IR camera image of the heater, the driving voltage is 7 V. **c** Temperature evolution of the FTH as a function of applied voltages ranging from 1 to 7 V. **d** On/off responses over 5 cycles under an DC bias voltage of 5 V



of the FTH based on the Ag NWs/PEDOT:PSS hybrid thin films. This fast temperature response suggests that our FTH may be feasible to applications such as automobile window defrosters that require fast temperature switching.

4 Conclusions

In summary, we develop a simple method to demonstrate cohesively improved figure of merit and adhesion of Ag NW based flexible transparent electrodes on low-cost PET substrate without vacuum process. On one hand, the PEDOT:PSS bond the Ag NWs tightly on the PET substrate. The adhesion improvement of Ag NW to PET substrate in turn enhanced the conductivity because of the downward force exerted by the PEDOT:PSS adhesive gel on Ag NWs. On the other hand, the PEDOT:PSS provides a significant electronic transmission channel between Ag NWs, leading to the further increase of conductivity. As a result, a high figure of merit (340) in Ag NW networks is obtained, while the sheet resistance is 9.4 Ω /sq at transmittance of 89.2%. The F value is superior to that obtained from the flexible ITO, carbon nanotube, graphene, copper nanowire, and other silver nanowire and hybrid thin films. In addition, a conduction mechanism is proposed to elucidate the resistance variation with addition of PEDOT:PSS. Meanwhile, the sheet resistance does not show great change after tape test, suggesting a good adhesion and of Ag NW to the PET substrate. Meanwhile, the sheet resistance does not show great change after tape test and bending test. Finally, the successful implementation of the prepared Ag NW based transparent electrodes into a flexible transparent heater is demonstrated, verifying the applicability of the electrodes. It is believed that our findings not only provide an effective way for the production of low-cost and high-performance Ag NW-based FTCEs but also realize their widespread use in emerging electronic applications.

Acknowledgments This work was supported by the Natural Science Foundation of Tianjin City (Grant No. 18JCQNJC01300), National Natural Science Foundation of China (Grant Nos. 61701338, 61804105), National Key R.&D. Program of China (Grant No. 2017YFB0406300), Foundation (B) for Peiyang Scholar-Young Core Faculty of Tianjin University (Grant No. 2018XRG-0020), Fund for Shanxi '1331 Project' Key Subject Construction, Scientific Research Foundation for High-Level Talents (Innovative Team) of Dongguan University of Technology (Grant No. KCYCXPT2017003).

References

1. D. Li, W.Y. Lai, Y.Z. Zhang, W. Huang, Printable transparent conductive films for flexible electronics. *Adv. Mater.* **30**, 1704738 (2018)
2. S. Yu, W. Zhang, L. Li, H. Dong, D. Xu, Y. Jin, Structural, electrical, photoluminescence and optical properties of n-type conducting, phosphorus-doped ZnO thin films prepared by pulsed laser deposition. *Appl. Surf. Sci.* **298**, 44–49 (2014)
3. S. Yu, L. Zhao, R. Liu, C. Zhang, H. Zheng, Y. Sun, L. Li, Performance enhancement of Cu-based AZO multilayer thin films via graphene fence engineering for organic solar cells. *Sol. Energy Mater. Sol. Cells* **183**, 66–72 (2018)
4. S. Walia, R. Gupta, K.D.M. Rao, G.U. Kulkarni, Transparent Pd wire network-based areal hydrogen sensor with inherent joule heater. *ACS Appl. Mater. Inter.* **8**, 23419–23424 (2016)
5. S. Yu, W. Zhang, L. Li, D. Xu, H. Dong, Y. Jin, Transparent conductive Sb-doped SnO₂/Ag multilayer films fabricated by magnetron sputtering for flexible electronics. *Acta Mater.* **61**, 5429–5436 (2013)
6. Y. Song, S. Chang, S. Gradecak, J. Kong, Visibly-transparent organic solar cells on flexible substrates with all-graphene electrodes. *Adv. Energy Mater.* **6**, 1600847 (2016)
7. I. Jeon, J. Yoon, N. Ahn, M. Atwa, C. Delacou, A. Anisimov, E.I. Kauppinen, M. Choi, S. Maruyama, Y. Matsuo, Carbon nanotubes versus graphene as flexible transparent electrodes in inverted perovskite solar cells. *J. Phys. Chem. Lett.* **8**(5395–540), 1 (2017)
8. L. Zhao, S. Yu, X. Li, M. Wu, L. Li, High-performance copper mesh transparent flexible conductors based on electroplating with vacuum-free processing. *Org. Electron.* **82**, 105511 (2020)
9. Y. Li, M. Wu, Y. Sun, S. Yu, High-performance flexible transparent conductive thin films on PET substrates with a CuM/AZO structure. *J. Mater. Sci. Mater. Electron.* **30**, 13271–13279 (2019)
10. M.N. Gueye, A. Carella, N. Massonnet, E. Yvenou, S. Brenet, J. Faure-Vincent, S. Pouget, F. Rieutord, H. Okuno, A. Benayad, R. Demadrille, J. Simonato, Structure and dopant engineering in PEDOT thin films: practical tools for a dramatic conductivity enhancement. *Chem. Mater.* **28**, 3462–3468 (2016)
11. L. Zhao, S. Yu, X. Li, M. Wu, L. Li, High-performance flexible transparent conductive films based on copper nanowires with electroplating welded junctions. *Sol. Energy Mater. Sol. Cells* **201**, 110067 (2019)
12. X. Liu, D. Li, X. Chen, W.Y. Lai, W. Huang, Highly transparent and flexible all-solid-state supercapacitors based on ultralong silver nanowire conductive networks. *ACS Appl. Mater. Inter.* **10**, 32536–32542 (2018)
13. M. Wu, H. Zheng, X. Li, S. Yu, Highly transparent low resistance ATO/AgNWs/ATO flexible transparent conductive thin films. *Ceram. Inter.* **46**, 4344–4350 (2020)
14. W. Jo, H.S. Kang, J. Choi, H. Lee, H.T. Kim, Plasticized polymer interlayer for low-temperature fabrication of a high-quality silver nanowire-based flexible transparent and conductive film. *ACS Appl. Mater. Inter.* **9**, 15114–15121 (2017)
15. Y. Jin, K. Wang, Y. Cheng, Q. Pei, Y. Xu, F. Xiao, Removable large-area ultrasoft silver nanowire transparent composite electrode. *ACS Appl. Mater. Inter.* **9**, 4733–4741 (2017)
16. H. Koseoglu, F. Turkoglu, M. Kurt, M.D. Yaman, F.G. Akca, G. Aygun, L. Ozyuzer, Improvement of optical and electrical properties of ito thin films by electro-annealing. *Vacuum* **120**, 8–13 (2015)
17. O. Tuna, Y. Selamet, G. Aygun, L. Ozyuzer, High quality ito thin films grown by dc and rf sputtering without oxygen. *J. Phys. D: Appl. Phys.* **43**, 055402 (2010)
18. S. Cho, S. Kang, A. Pandya, R. Shanker, Z. Khan, Y. Lee, J. Park, S.L. Craig, H. Ko, Large-area cross-aligned silver nanowire electrodes for flexible, transparent, and force-sensitive mechanochromic touch screens. *ACS Nano* **11**, 4346–4357 (2017)
19. Y.R. Jang, W.H. Chung, Y.T. Hwang, H.J. Hwang, S.H. Kim, H.S. Kim, Selective wavelength plasmonic flash light welding of silver nanowires for transparent electrodes with high conductivity. *ACS Appl. Mater. Inter.* **10**, 24099–24107 (2018)

20. Y. Huang, S. Liao, J. Ren, B. Khalid, H. Peng, H. Wu, A transparent, conducting tape for flexible electronics. *Nano Res.* **9**, 917–924 (2016)
21. K.W. Seo, J.H. Lee, H.J. Kim, H.K. Kim, S.I. Na, Highly transparent and flexible intio/Ag nanowire/intio films for flexible organic solar cells. *Appl. Phys. Lett.* **105**, 031911 (2014)
22. H. Sohn, S. Kim, W. Shin, J.M. Lee, H. Lee, D.J. Yun, K.S. Moon, I.T. Han, C. Kwak, S.J. Hwang, Novel flexible transparent conductive films with enhanced chemical and electromechanical sustainability: TiO₂ nanosheet-Ag nanowire hybrid. *ACS Appl. Mater. Inter.* **10**, 2688–2700 (2018)
23. J. Han, S. Yuan, L. Liu, X. Qiu, H. Gong, X. Yang, C. Li, Y. Hao, B. Cao, Fully indium-free flexible Ag nanowires/ZnO: F composite transparent conductive electrodes with high haze. *J. Mater. Chem. A* **3**, 5375–5384 (2015)
24. Y.H. Kim, C. Sachse, M.L. Machala, C. May, L. Müller-Meskamp, K. Leo, Highly conductive PEDOT: PSS electrode with optimized solvent and thermal post-treatment for ITO-free organic solar cells. *Adv. Funct. Mater.* **21**, 1076–1081 (2011)
25. Y.S. Kim, E.J. Lee, J.T. Lee, D.K. Hwang, W.K. Choi, J.Y. Kim, High-performance flexible transparent electrode films based on silver nanowire-PEDOT: PSS hybrid-gels. *RSC Adv.* **6**(69), 64428–64433 (2016)
26. T. Kim, S. Park, J. Seo, C.W. Lee, J.M. Kim, Highly conductive PEDOT: PSS with enhanced chemical stability. *Org. Electron.* **74**, 77–81 (2019)
27. Q. Zhang, Y. Lu, Z. Liu, H. Yu, Y. Duan, L. Liu, S. Chen, W. Huang, Highly efficient organic-inorganic hybrid perovskite quantum dot/nanocrystal light-emitting diodes using graphene electrode and modified PEDOT: PSS. *Org. Electron.* **72**, 30–38 (2019)
28. L. Hu, D.S. Hecht, G. Grüner, Percolation in transparent and conducting carbon nanotube networks. *Nano Lett.* **4**, 2513–2517 (2004)
29. S. De, T.M. Higgins, P.E. Lyons, E.M. Doherty, P.N. Nirmalraj, W.J. Blau, J.J. Boland, J.N. Coleman, Silver nanowire networks as flexible, transparent, conducting films: extremely high dc to optical conductivity ratios. *ACS Nano* **3**, 1767–1774 (2009)
30. V. Nam, D. Lee, Copper nanowires and their applications for flexible, transparent conducting films: a review. *Nanomaterials* **6**, 47 (2016)
31. H.J. Choi, S.G. Yoon, J.H. Lee, J.Y. Lee, Crystallized indium–tin oxide (ITO) thin films grown at low temperature onto flexible polymer substrates. *ECS J. Solid State Sc. Technol.* **1**, Q106–Q109 (2012)
32. M.H. Ahn, E.S. Cho, S.J. Kwon, Characteristics of ITO–resistive touch film deposited on a pet substrate by in-line dc magnetron sputtering. *Vacuum* **101**, 221–227 (2014)
33. C. Feng, K. Liu, J.S. Wu, L. Liu, J.S. Cheng, Y.Y. Zhang, Y.H. Sun, Q.Q. Li, S.S. Fan, K.L. Jiang, Flexible, stretchable, transparent conducting films made from superaligned carbon nanotubes. *Adv. Funct. Mater.* **20**, 885–891 (2010)
34. J. Kang, H. Kim, K.S. Kim, S.K. Lee, S. Bae, J.H. Ahn, Y.J. Kim, J.B. Choi, B.H. Hong, High-performance grapheme-based transparent flexible heaters. *Nano Lett.* **11**, 5154–5158 (2011)
35. Y. Jin, L. Li, Y. Cheng, L. Kong, Q. Pei, F. Xiao, Cohesively enhanced conductivity and adhesion of flexible silver nanowire networks by biocompatible polymer sol–gel transition. *Adv. Funct. Mater.* **25**, 1581–1587 (2015)
36. T. He, A. Xie, D.H. Reneker, Y. Zhu, A tough and high-performance transparent electrode from a scalable and transfer-free method. *ACS Nano* **8**, 4782–4789 (2014)
37. S. Han, S. Hong, J. Ham, J. Yeo, J. Lee, B. Kang, P. Lee, J. Kwon, S.S. Lee, M.Y. Yang, S.H. Ko, Fast plasmonic laser nanowelding for a Cu-nanowire percolation network for flexible transparent conductors and stretchable electronics. *Adv. Mater.* **26**, 5808–5814 (2014)
38. X. Li, H. Wang, Q. Xu, S. Guo, J. Du, X. Liu, J. Weng, J. Xu, Ultrathin AuAg nanofilms from ice-templated assembly of AuAg nanowires. *Adv. Mater. Inter.* **5**, 1800256 (2018)
39. T. Kim, A. Canlier, C. Cho, V. Rozyyev, J.Y. Lee, S.M. Han, Highly transparent Au-coated Ag nanowire transparent electrode with reduction in haze. *ACS Appl. Mater. Inter.* **6**, 13527–13534 (2014)
40. D. Lee, H. Lee, Y. Ahn, Y. Lee, High-performance flexible transparent conductive film based on graphene/AgNW/graphene sandwich structure. *Carbon* **81**, 439–446 (2015)
41. A.L. Gorkina, A.P. Tsapenko, E.P. Gilshteyn, T.S. Koltsova, T.V. Larionova, A. Talyzin, A.S. Anisimov, I.V. Anoshkin, E.I. Kauppinen, O.V. Tolochko, A.G. Nasibulin, Transparent and conductive hybrid graphene/carbon nanotube films. *Carbon* **100**, 501–507 (2016)
42. K.H. Choi, J. Kim, Y.J. Noh, S.I. Na, H.K. Kim, Ag nanowire-embedded ITO films as a near-infrared transparent and flexible anode for flexible organic solar cells. *Sol. Energy Mater. Sol. Cells* **110**, 147–153 (2013)
43. K.A. Nagamatsu, S. Avasthi, J. Jhaveri, J.C. Sturm, Efficient silicon/PEDOT: PSS heterojunction solar cell fabricated at 300 °C. *IEEE J. Photovolt.* **4**, 260–264 (2014)
44. A.M. Nardes, M. Kemerink, M.M. De Kok, E. Vinken, K. Maturova, R.A.J. Janssen, Conductivity, work function, and environmental stability of PEDOT: PSS thin films treated with sorbitol. *Org. Electr.* **9**, 727–734 (2008)
45. J. Jin, J. Lee, S. Jeong, S.C. Yang, J.H. Ko, H.G. Im, S.W. Baek, J.Y. Lee, B.S. Bae, High-performance hybrid plastic films: a robust electrode platform for thin-film optoelectronics. *Energy Environ. Sci.* **6**, 1811–1817 (2013)
46. Y. Lee, S.Y. Min, T.W. Lee, Large-scale highly aligned nanowire printing. *Macromol. Mater. Eng.* **302**, 1600507 (2017)
47. S.I. Park, J.H. Ahn, X. Feng, S. Wang, Y. Huang, J.A. Rogers, Theoretical and experimental studies of bending of inorganic electronic materials on plastic substrates. *Adv. Funct. Mater.* **18**, 2673–2684 (2008)
48. T.B. Song, Y. Chen, C.H. Chung, Y. Yang, B. Bob, H.S. Duan, G. Li, K.N. Tu, Y. Huang, Y. Yang, Nanoscale joule heating and electromigration enhanced ripening of silver nanowire contacts. *ACS Nano* **8**, 2804–2811 (2014)
49. F. Wang, C. Gao, K. Kuklane, I. Holmér, A review of technology of personal heating garments. *Int. J. Occup. Saf. Ergon.* **16**, 387–404 (2010)

Publisher's Note Springer Nature remains neutral with regard to jurisdictional claims in published maps and institutional affiliations.